Geometrical and electronic structure of the Ba-doped Sin (n = 1–12) cluster: A density functional study

ARTICLE *in* JOURNAL OF MOLECULAR STRUCTURE · OCTOBER 2014

Impact Factor: 1.6 · DOI: 10.1016/j.molstruc.2014.06.089

5 AUTHORS, INCLUDING:

Zhang Shuai
Nanyang Normal University
19 PUBLICATIONS **18** CITATIONS
SEE PROFILE

Cheng Lu
Nanyang Normal University
46 PUBLICATIONS **111** CITATIONS
SEE PROFILE

Journal of Molecular Structure 1075 (2014) 220–226

Contents lists available at ScienceDirect

Journal of Molecular Structure

journal homepage: www.elsevier.com/locate/molstruc

Geometrical and electronic structure of the Ba-doped Si_n (n = 1–12) cluster: A density functional study

Shuai Zhang [a], Wei Dai [b], Hongzhao Liu [a], Cheng Lu [a,c,d,*], Genquan Li [a]

[a] Department of Physics, Nanyang Normal University, Nanyang 473061, China
[b] School of Physics and Mechanical & Electronical Engineering, Hubei University of Education, Wuhan 430205, China
[c] State Key Laboratory of Superhard Materials, Jilin University, Changchun 130012, China
[d] Beijing Computational Science Research Center, Beijing 100084, China

HIGHLIGHTS

- The geometric structures of $BaSi_n$ and Si_{n+1} (n = 1–12) clusters are determined.
- The stabilities and electronic properties of $BaSi_n$ clusters are discussed.
- The $BaSi_n$ (n = 2, 5, 8) have the higher stability than other clusters.
- The charges in $BaSi_n$ clusters transfers from the Ba atom to Si atom.

ARTICLE INFO

Article history:
Received 2 May 2014
Received in revised form 17 June 2014
Accepted 27 June 2014
Available online 5 July 2014

Keywords:
Geometrical structure
Electronic structure
Density functional theory
Ba-doped Si_n cluster

ABSTRACT

The structures, stabilities and electronic properties of $BaSi_n$ and Si_{n+1} (n = 1–12) clusters are systematically studied by density functional calculations using the B3LYP exchange–correlation potential. Extensive structure search based on large numbers of initial configurations has been carried out to identify the stable isomers of $BaSi_n$ (n = 1–12) clusters. We found that the most stable isomers of $BaSi_n$ clusters are three-dimensional structures when n > 3, and the most stable structures of $BaSi_n$ clusters often can be created by adding Ba or substituting Si by Ba in pure silicon clusters. The stability has been analyzed based on the average binding energy, fragmentation energy and second-order energy difference. The calculated results indicate that $BaSi_n$ clusters with n = 2, 5, 8 and 10 have higher stability than other clusters. The analysis of the highest occupied molecular orbital and the lowest unoccupied molecular orbital suggests that the substitution of Ba atom reduce the gaps of the Si_{n+1} clusters. The Mulliken populations of the Ba atom in the $BaSi_n$ clusters vary from 0.506 to 1.574, showing that the charges in $BaSi_n$ clusters transfers from the Ba atom to Si atoms. Furthermore, the vertical ionization potential, vertical electron affinity, chemical hardness, infrared and Raman spectra are also analyzed.

Introduction

The experimental and theoretical studies of the atomic and molecular clusters are interesting topics [1–6], since these clusters constitute intermediate phases between atom and bulk phases, which can be used to understand how physical properties and structures evolve from atoms and molecules to the bulk phase. The research on the silicon-based clusters is of particular interest, due to their numerous technological applications and the intensive ongoing efforts to reduce sizes in nanomaterials [7–9]. In current semiconductor industry, nanoelectronic devices are often fabricated by lithographic techniques. To generate cluster-assembled nanostructures, it is important to obtain proper building blocks that are chemically stable and weakly interact with each other. Inspired by wide application of Si materials in semiconductor industry and the well development of silicon based technology, silicon clusters have been intensively researched as such building blocks. However, pure silicon clusters are often chemically unstable due to the existence of dangling bonds. Doping silicon clusters with metal atoms is a possible way to stabilize the silicon clusters. Furthermore, introducing metal atoms in silicon clusters can effectively modify the geometry and electronic properties.

Many metal-doped silicon clusters have been studied in great detail by numerous experimental and theoretical works. Using X-

* Corresponding author at: Department of Physics, Nanyang Normal University, Nanyang 473061, China.
E-mail address: lucheng@calypso.cn (C. Lu).

http://dx.doi.org/10.1016/j.molstruc.2014.06.089
0022-2860/

ray absorption spectroscopy, Lau et al. [10] investigated the electronic and geometric properties of $TiSi_{16}^{+}$, VSi_{16}^{+} and $CrSi_{16}^{+}$ clusters and revealed that electronic and geometric properties are correlated in highly symmetric clusters. Based on the anion photoelectron spectroscopy and density functional theory calculations, Kong et al. [11] investigated Cr-doped silicon clusters and found that the endohedral structure for $CrSi_n^-$ clusters emerged at $n = 10$ and the magnetic properties of the clusters could be correlated to their geometry. Grubisic et al. [12] measured the photoelectron spectra of $EuSi_n^-$ $(3 \leqslant n \leqslant 17)$ cluster anions. The evolution of the photoelectron spectra of $EuSi_n^-$ clusters with size n reveals a major change in their electronic structure over the size range $n = 10$–12. In order to elucidate the growth behavior of the Eu-doped Si clusters, Zhao et al. [13] studied the geometries, stabilities, electronic and magnetic properties of the europium encapsulated $EuSi_n$ ($n = 1$–13) clusters by using relativistic density functional theory (DFT) with the generalized gradient approximation (GGA) at PW91 level. By using first-principles DFT-GGA approach, Guo et al. [14] reported the theoretical investigations on the stabilities, and magnetic properties of the transition metal encapsulated MSi_n (M = Sc, Ti, V, Cr, Mn, Fe, Co, Ni, Cu, Zn; $n = 8$–16) clusters.

Barium is the most lively alkali-earth metal element with rich physical and chemical properties, it is not only can be used as degasifying agent/degassing, but also be employed an important alloying element. Although metal doped silicon clusters have been extensively studied in recent years [12–14], there is no systematic theoretical and experimental investigation on $BaSi_n$ clusters. In order to gain insight into the geometries and electronic properties of the $BaSi_n$ clusters and further enrich our knowledge of silicon-based clusters, we carried out the computational studies on a series of $BaSi_n$ ($n = 1$–12) clusters and compared with that of pure Si_{n+1} clusters. Our first goal is to gain a fundamental understanding of the ground state geometric structures in $BaSi_n$ ($n = 1$–12) clusters. The second goal is to further explore the physical mechanism of the growth behaviors of $BaSi_n$ clusters. Thirdly, we are also motivated to seek the correlation between geometry, electronic structures, and properties of alkaline-earth metal doped silicon clusters in general.

Computational details

All the geometry optimizations of the pure Si_{n+1} and $BaSi_n$ ($n = 1$–12) clusters have been carried out by using the B3LYP method [15] in the Gaussian 09 program package [16]. By taking the time-consumption into account, the basis sets labelled GENECP are the combinations of pseudopotential with basis sets LANL2DZ and full electrons basis sets 6-311+G(d), which are employed for the Ba and Si atoms, respectively. To search the lowest-energy structures, a large number of previous optimized Si_n and XSi_n geometries [17–24] are considered as our initial structures. Then, we constructed many structures by placing one Ba atom at each possible sites on the basis of initial structures, i.e., Ba-capped, Ba-substituted, and Ba-encapsulated patterns. For the $BaSi_n$ clusters, three different spin multiplicities (singlet, triplet and quintet) are considered owing to the spin polarization [25]. Once the imaginary vibrational mode is discovered, a relaxation is rearranged along the coordinates of the imaginary vibrational mode until the local minimum is obtained. In order to test the reliability of the calculation method, we first performed a comparison by employing different density functional for small clusters BaSi, Ba_2 and Si_2. The results as well as the experimental data are listed in Table 1. From the table, we can see that the theoretical results of Si_2 based on the B3LYP functional are in good agreement with the experimental and theoretical values [26,30]. The calculated bond length, vibrational frequency, and fragmentation energy are 3.44 Å, 138.7 cm^{-1}, 0.83 eV for BaSi and 4.71 Å, 51.9 cm^{-1}, 1.32 eV for Ba_2, respectively. These calculated results are in accord with the similar theoretical results of 3.46 Å for the bond length of Ba–Si and 4.75/4.72 Å for the bond length of Ba–Ba [27–29]. The good agreement between them shows the accuracy of the present theoretical calculations.

Results and discussions

Bare silicon cluster Si_n ($n = 3$–13)

We first optimized the structures of pure silicon clusters Si_{n+1} ($n = 3$–13) clusters by using the identical method and basis set. The lowest-energy structures are shown in Fig. 1. As shown in Fig. 1, the ground state structures of Si_{n+1} ($n > 4$) clusters favor sp^3-like bonding and forms three-dimensional (3D) structures, in contrast to carbon clusters that favor sp^2-like bonding and tend to form linear or planar cyclic structures.

Barium-doped silicon cluster $BaSi_n$ ($n = 1$–12)

Although large numbers of clusters are studied in this work, only the lowest-energy and a few low-lying isomers are shown in Figs. 2 and 3. These isomers are denoted by their energy orders from low to high as *n*a, *n*b, *n*c and *n*d (*n* is the number of Si atoms in $BaSi_n$ clusters). Meanwhile, the symmetry, electronic state, lowest and highest vibrational frequencies, highest occupied molecule orbital (HOMO) and lowest unoccupied molecule orbital (LUMO) energies are summarized in Table 2.

The diatomic BaSi cluster with $C_{\infty v}$ symmetry is optimized. The calculated results show that the triplet spin state is the lowest among all possible spin states. Hence, the triplet BaSi dimer with electronic state of $^3\sum$ is the ground state structure. This configuration is similar to previous TMSi (TM = W, Mo, Fe and Ag) [31–34], which have the most stable structures with a spin triplet or quintet configuration. The bond length of triplet BaSi dimer is 3.44 Å, which is longer than that of Si–Si (2.28 Å). This result can be attributed to the closed s-shell of the electronic configuration for the Ba atom and the weaker Ba–Si interaction. The possible structures of $BaSi_2$ such as C_{2v}, $C_{\infty v}$ and $D_{\infty h}$ isomers are optimized as the stable geometries. The most stable isomer is an isosceles triangle structure (2a) with C_{2v} symmetry, 38.27° angel of Si–Ba–Si and 3.35 Å of the bond length Ba–Si. The linear structure 2b ($C_{\infty v}$) with Ba atom at one end is 0.25 eV higher in energy than the 2a isomer. For $BaSi_3$, the lowest-energy structure 3a and the other two different low-lying isomers 3b and 3c are obtained within an energy range of 0.49 eV. The most stable isomer 3a with one Ba atom occupying the vertex of the triangular pyramid is an irregular triple prism structure. The calculated results show that the 3a is lower in total energy than 3b, and 3c by 0.14 and 0.49 eV, respectively. For $n = 4$, the most stable isomer (4a) is a 3D structure with $^1A'$ state and C_s symmetry. It can be viewed as one Ba atom replacing one Si atom on one side of a pyramidic Si_5 cluster. Similar to the configuration of the lowest-energy Si_6 [23] cluster, the tetragonal bipyramid 5a isomer is the ground-state structure of $BaSi_5$ clusters. The second isomer 5b (C_1) is a triangular prism structure, which is 0.13 eV higher than that of lowest-energy isomer 5a. According to the calculated total energies of the four $BaSi_6$ isomers, isomer 6a is proved to be the lowest-energy structure. It can be seen as one of pentagonal bipyramid with Ba atom on the base. The similar site preference is also found in the ground state structures of NSi_6 [35] and PSi_6 [36] clusters. For $BaSi_7$, the ground state isomer, 7a, with C_1 symmetry is generated by capping the lowest-energy structure Si_7 with one Ba atom. As for the $BaSi_8$ cluster, on the basis

Table 1
Calculated, experimental and theoretical bond lengths (r), dissociation energies (D) and frequencies (ω) of the BaSi, Ba_2 and Si_2 clusters.

Methods	BaSi			Ba_2			Si_2		
	r (Å)	ω (cm^{-1})	D (eV)	r (Å)	ω (cm^{-1})	D (eV)	r (Å)	ω (cm^{-1})	D (eV)
PW91PW91	3.39	149.6	1.15	4.64	53.8	0.95	2.30	468.72	3.38
PBEPBE	3.39	148.3	1.13	4.65	53.7	0.97	2.30	468.76	3.37
BP86	3.40	145.7	1.06	4.66	52.6	1.09	2.30	465.6	3.37
B3LYP	3.44	138.7	0.83	4.71	51.9	1.32	2.28	485.5	3.06
Experiment	–	–	–	–	–	–	2.25[a]	511.0[a]	3.22[a]
Theory	3.46[b]	–	–	4.75[c] 4.72[d]	–	–	2.29[e]	494[e]	–

[a] Ref. [26].
[b] Ref. [27].
[c] Ref. [28].
[d] Ref. [29].
[e] Ref. [30].

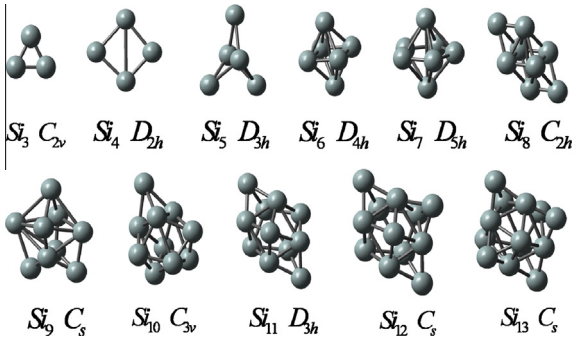

Fig. 1. The lowest-energy structure of Si_n (n = 3–13) clusters.

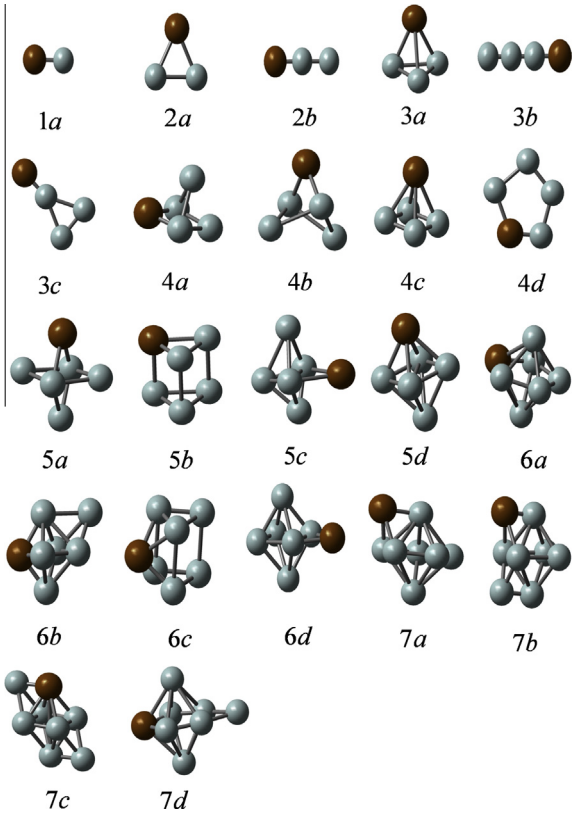

Fig. 2. The lowest-energy and low-lying isomers for $BaSi_n$ (n = 1–7) clusters. The light and brown balls represent Si and Ba atoms, respectively. (For interpretation of the references to colour in this figure legend, the reader is referred to the web version of this article.)

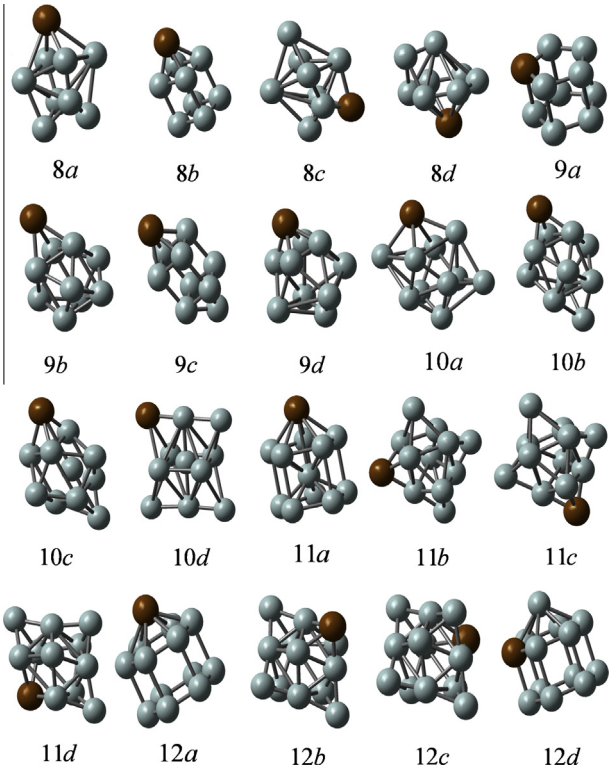

Fig. 3. The lowest-energy and low-lying isomers for $BaSi_n$ (n = 8–12) clusters. The light and brown balls represent Si and Ba atoms, respectively. (For interpretation of the references to color in this figure legend, the reader is referred to the web version of this article.)

of the Si_9, one substituted isomer 8a can be obtained when one Si atom of the lowest-energy Si_9 cluster is substituted by one Ba atom. After one Ba atom capped the top of the hexahedron Si_8, the second isomer 8b is obtained. The third isomer 8c is similar to the geometry of isomer 8a. However, the energy of 8c is higher than that of 8a by 0.57 eV. When n = 9, the isomer 9a with C_1 symmetry is found to be the most stable structure, which is a pentagonal prism structure. The other three low-lying isomers (9b, 9c and 9d) are presented in Fig. 3. The calculated results indicate that the isomer 9a is lower in energy by 0.11, 0.48 and 0.61 eV than isomers 9b, 9c and 9d, respectively. For $BaSi_{10}$ cluster, the isomer 10a, with C_1 symmetry, is the lowest structure. It can be viewed as the low-lying structure of $BaSi_9$ (9d) being capped by one Si atom. For $BaSi_{11}$ clusters, the lowest-energy isomer (11a) is identified as one Ba atom capping on the top of a Si-centered pentagonal prism Si_{11}. When the number of $BaSi_n$ cluster is up to 12, the isomer 12a

Table 2
The symmetries, electronic states, frequency (cm^{-1}), HOMO and LUMO energies (a.u.) of $BaSi_n$ (n = 1–12) clusters.

	Sta	Sym	Frequency		HOMO	LUMO		Sta	Sym	Frequency		HOMO	LUMO
			Lowest	Highest						Lowest	Highest		
1a	$^3\Sigma$	$C_{\infty v}$		138.70	−0.15400	−0.06952	7d	$^3B_1$	C_{2v}	41.21	486.54	−0.15396	−0.11110
2a	$^1A_1$	C_{2v}	110.28	510.17	−0.15557	−0.11168	8a	$^1A'$	C_s	65.58	449.39	−0.16703	−0.13255
2b	==	$C_{\infty v}$	57.82	571.86	−0.14956	−0.10872	8b	$^3B_1$	C_{2v}	41.52	439.04	−0.15599	−0.13566
3a	$^1A'$	C_s	46.15	426.96	−0.13804	−0.12476	8c	$^1A'$	C_s	52.94	513.99	−0.16824	−0.11785
3b	^3A	C_1	35.66	559.41	−0.15501	−1.35355	8d	^1A	C_1	65.43	500.54	−0.16732	−0.11680
3c	^5A	C_1	21.32	384.80	−0.15532	−0.14123	9a	^1A	C_1	24.58	472.12	−0.16382	−0.11453
4a	$^1A'$	C_s	51.12	457.26	−0.15522	−0.11456	9b	^1A	C_1	57.69	392.32	−0.17522	−0.12978
4b	$^3B_1$	C_{2v}	29.15	448.53	−0.15967	−0.11438	9c	^3A	C_1	36.12	493.50	−0.15796	−0.11497
4c	$^1A_1$	C_{2v}	46.92	704.90	−0.14690	−0.12904	9d	^3A	C_1	56.20	410.20	−0.17206	−0.12688
4d	^3A	C_1	64.81	546.34	−0.15220	−0.11165	10a	^1A	C_1	38.10	418.65	−0.17942	−0.12394
5a	$^1A'$	C_s	46.87	453.06	−0.16877	−0.11977	10b	^1A	C_1	38.48	446.87	−0.16484	−0.10852
5b	^1A	C_1	47.29	453.88	−0.16887	−0.11976	10c	^3A	C_1	9.59	496.68	−0.15371	−0.12470
5c	$^3A'$	C_s	30.09	477.33	−0.15405	−0.14662	10d	^1A	C_1	61.29	494.10	−0.16353	−0.12754
5d	$^3A_2$	C_{2v}	85.68	424.97	−0.15744	−0.11363	11a	^1A	C_1	10.33	481.12	−0.17036	−0.11233
6a	$^3A''$	C_s	43.32	426.46	−0.15388	−0.11894	11b	^1A	C_1	30.31	488.68	−0.16367	−0.12085
6b	^3A	C_1	29.29	449.39	−0.15566	−0.10699	11c	^3A	C_1	35.11	459.39	−0.15253	−0.12658
6c	$^3A'$	C_s	49.80	461.40	−0.15278	−0.10880	11d	$^3A'$	C_s	46.90	472.82	−0.15735	−0.12125
6d	$^5A''$	C_s	15.30	435.68	−0.14757	−0.12566	12a	^1A	C_1	87.87	465.37	−0.19017	−0.12959
7a	^1A	C_1	35.19	396.99	−0.15471	−0.10947	12b	$^1A'$	C_s	40.66	496.67	−0.17108	−0.12565
7b	^3A	C_1	34.76	395.79	−0.15639	−0.10965	12c	$^1A'$	C_s	59.75	483.55	−0.17913	−0.11463
7c	$^3A'$	C_s	23.76	480.39	−0.15321	−0.11998	12d	^1A	C_1	57.47	559.68	−0.17384	−0.10789

is optimized to be the most stable structure. It is obtained after one Si atom is capped on the top of the hexagonal prism Si_{12}, The isomers 12b and 12c are two substituted geometries, in which the Ba atom replace different Si atom of C_s Si_{13} cluster. The low-lying isomers 12b, 12c, and 12d lie above the lowest-energy isomer 12a by 0.34, 0.49, and 0.51 eV, respectively.

According to the above discussions, we find that the ground state structures of $BaSi_n$ clusters favor the 3D structures for n = 3–12 and planar structures for n = 1–2. When $n \leqslant 6$, the growth pattern can be viewed as being derived from Si_{n+1} by replacing one Si atom with one Ba atom. This results are similar to the previous reports of XSi_n (X = Be, Li, K, Mg and Ca) clusters [8,37–40]. For $n > 6$, the growth behavior is the"capping structure", in which the Si capping of $BaSi_{n-1}$ clusters and Ba capping of Si_n clusters. However, the lowest-energy structures do not include any structure containing Si cages encapsulating Ba. This is different from the other metal doped silicon clusters, especially for transition metal, in which the metal atom occupies the center of the silicon clusters [41–43]. But, it is similar to the alkali metal doped Si clusters, such as $LiSi_n$, in which the Li atom favors adsorption on an edge or a face of Si_n cluster [44]. The results reveal that the location of the impurity atom depends on the nature of interaction between the impurity atom and the host cluster.

Relative stabilities

In order to gain insight into the relative stabilities of the $BaSi_n$ clusters, the averaged binding energy $E_b(n)$, fragmentation energy $D(n)$, and second-order energy difference $\Delta_2E(n)$ are calculated. The $E_b(n)$ of $BaSi_n$ and Si_{n+1} clusters can be defined as [45]

$$E_b(n+1) = [(n+1)E_k(\mathrm{Si}) - E_k(\mathrm{Si}_{n+1})]/(n+1) \quad (1)$$

$$E_b(n) = [nE_k(\mathrm{Si}) + E_k(\mathrm{Ba}) - E_k(\mathrm{BaSi}_n)]/(n+1) \quad (2)$$

where E_k(Si), E_k(Ba), $E_k(Si_{n+1})$ and E_k(BaSi) represents the total energy of the Si atom, Ba atom, the most stable Si_{n+1} and $BaSi_n$ clusters, respectively.

Fig. 4(a) shows the size dependence of $E_b(n)$ for the lowest-energy $BaSi_n$ and pure Si_{n+1} clusters. From Fig. 4(a), we can see that the $E_b(n)$ of Si_{n+1} and $BaSi_n$ clusters gradually increase with increasing cluster size. In addition, the $E_b(n)$ of the $BaSi_n$ clusters are smaller than those of the pure Si_{n+1} clusters. This character indicates that the impurity Ba atom can enhance the chemical activity of silicon cluster [42].

The fragmentation energy $D(n)$ and second-order energy difference $\Delta_2E(n)$ can be expressed as the following formulas [46]

$$D(n) = E_k(\mathrm{BaSi}_{n-1}) + E_k(\mathrm{Si}) - E_k(\mathrm{BaSi}_n) \quad (3)$$

$$\Delta_2E(n) = E_k(\mathrm{BaSi}_{n+1}) + E_k(\mathrm{BaSi}_{n-1}) - 2E_k(\mathrm{BaSi}_n) \quad (4)$$

where E_k represents the total energy. For the most stable $BaSi_n$ clusters, the size dependence of $D(n)$ and $\Delta_2E(n)$ are plotted in Fig. 4(b). The primary features are concluded as following: (i) the curves of $D(n)$ and $\Delta_2E(n)$ for $BaSi_n$ clusters show irregular oscillating behaviors, and the two curves almost have the same tendency. (ii) four visible peaks of $D(n)$ are found at n = 2, 5, 8 and 10, implying that the $BaSi_2$, $BaSi_5$, $BaSi_8$ and $BaSi_{10}$ clusters are more stable than their neighboring clusters. (iii) four local prominent maxima of $\Delta_2E(n)$ appear at the size of 2, 5, 8 and 10, suggesting that these clusters are relatively more stable than the others, which are consistent with the maxima presented in the $D(n)$.

HOMO–LUMO gaps and charge transfer

The HOMO–LUMO energy gaps E_{gap} (the energy gaps between the highest occupied molecular orbital (HOMO) and lowest unoccupied molecular orbital (LUMO)) represents, to some extend, the ability of molecule to participate in chemical reactions. In general, a larger E_{gap} corresponds to a closed-shell electronic configuration with low chemical activity [47]. The size dependence of the E_{gap} for the ground state $BaSi_n$ and pure Si_{n+1} clusters are displayed in Fig. 4(c). It can be seen from Fig. 4(c) that the E_{gap} of $BaSi_{2,3,4,6,8,9,10,11}$ clusters are lower than those of $BaSi_{1,5,7,12}$ clusters. In other words, the $BaSi_{1,5,7,12}$ clusters have an enhanced chemical stability compared to their neighbors. Considering the trends of E_{gap}, $D(n)$ and $\Delta_2E(n)$, we can conclude that the most stable Ba doped Si cluster is $BaSi_5$. In addition, as shown in Fig. 4(c), the E_{gap} of $BaSi_n$ clusters are smaller than those of the Si_{n+1} clusters with an exception of BaSi. This fact confirms that doping Ba atoms does not enhance the chemical stability of silicon clusters, which is in accord with the above analysis of $E_b(n)$.

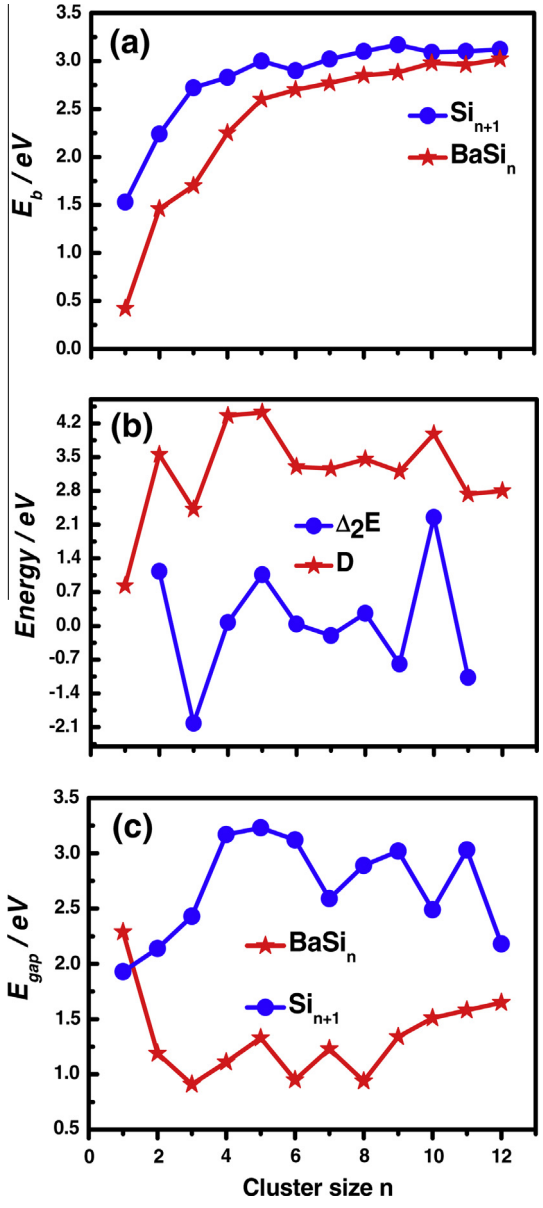

Fig. 4. Size dependence of the averaged binding energy $E_b(n)$, fragmentation energy $D(n)$, second-order energy difference $\Delta_2E(n)$ and HOMO–LUMO energy gaps E_{gap} for the lowest-energy structures of $BaSi_n$ and Si_{n+1} clusters.

In order to provide detailed information on the charge transfer of $BaSi_n$ clusters, the Mulliken Population (MP) analysis of the most stable $BaSi_n$ clusters has been calculated. The results are summarized in Table 3. As shown in Table 3, we can clearly see that the atomic charges of the Ba atom in the $BaSi_n$ clusters possess positive charges from 0.506 to 1.574 e. This is consistent to the expectation that the charges always transfers from Ba atom to Si atom, i.e., Ba acts as electron donor in all $BaSi_n$ clusters. This result may be caused by the electronegativity of Si (1.90) is much bigger than Ba (0.89) [48] and Ba has a stronger ability to lose electron.

Electrostatic potential

The electrostatic potential (ESP) created by the nuclei and electrons of a molecule in the surrounding space is well established as a guide to the interpretation and prediction of molecular behavior. Here, we computed the electrostatic potential by using self-consistent-field (SCF) molecular orbital methods. The electrostatic potential $V(r)$ can be calculated rigorously from its electron density $\rho(r)$, distribution by the equation [49]

$$V(\boldsymbol{r}) = \sum_A \frac{Z_A}{|\boldsymbol{R}_A - \boldsymbol{r}|} - \int \frac{\rho(\boldsymbol{r}')}{|\boldsymbol{r}' - \boldsymbol{r}|} d\boldsymbol{r}' \quad (5)$$

where Z_A is the nuclear charge of atom A, located at $\boldsymbol{R}_A$, and $\rho(\boldsymbol{r})$ is the electron density. After calculations of the electron densities of these most stable $BaSi_n$ (n = 1–12) clusters, the electrostatic potentials are calculated by Multiwfn program [50]. The isopotential lines are shown in the Supporting Information. The color coded scale ranges from −0.1 to 0.1 V covering colors from blue to red, respectively. The potential smaller than −0.1 V is represented by blue; whereas potentials larger than 0.1 V are represented by red. This color scale allows us to precisely determine if a region in the molecule shows positive or negative potentials. As expected, potentials in the neighborhood of the nuclei are positive, therefore the electrostatic potential plane will show a red region when the atoms locate exactly on it. Because Si has larger electronegativity than Ba, most negative region of ESP appears in the vicinity of Si atom. The bold blue line corresponds to the van der Waals (vdW) surface (isosurface of electron density = 0.001 a.u., as defined by Bader) [51]. The areas enclosed by blue lines are internal region of the molecule and will not be concerned. From the isopotential lines, it is clear that Ba atom is positively charged, because the local vdW surface closed to Ba atom largely intersected solid. This is in good agreement with the above analysis that the Ba atoms possess positive charges based on the natural population analysis.

Vertical ionization potential, vertical electron affinity and chemical hardness

It is well known that the vertical ionization potential (*VIP*) and vertical electron affinity (*VEA*) are the two significant parameters of the electronic properties. Based on the optimized structures, the *VIP* and *VEA* are calculated by employing the following formulas [52,53]:

Table 3
Mulliken charge population of Ba atom in the lowest-energy $BaSi_n$ (n = 1–12) clusters.

Cluster	Ba	Si-1	Si-2	Si-3	Si-4	Si-5	Si-6	Si-7	Si-8	Si-9	Si-10	Si-11	Si-12
BaSi	0.506	−0.506											
$BaSi_2$	0.878	−0.439	−0.439										
$BaSi_3$	0.655	−0.418	−0.266	−0.029									
$BaSi_4$	0.924	0.002	−0.041	−0.041	−0.844								
$BaSi_5$	1.431	−0.785	−0.785	0.358	−0.038	−0.181							
$BaSi_6$	0.789	0.124	−0.002	0.002	0.124	−0.493	−0.540						
$BaSi_7$	0.945	−0.079	−0.079	−0.285	−0.080	−0.079	−0.080	−0.262					
$BaSi_8$	1.505	−0.725	0.556	0.556	−0.725	−0.077	−0.505	0.077	−0.506				
$BaSi_9$	1.273	−0.821	0.446	0.268	−1.267	−0.018	−0.174	−0.140	0.167	0.266			
$BaSi_{10}$	1.379	−0.440	−0.347	−0.108	−0.112	−0.444	0.781	−0.351	0.331	−0.349	−0.339		
$BaSi_{11}$	1.265	0.384	0.374	−0.285	0.109	−1.375	0.391	0.146	−0.286	0.109	0.375	−1.208	
$BaSi_{12}$	1.574	−0.371	−0.370	−0.559	−1.023	0.313	0.313	−1.029	0.314	−0.370	0.559	0.557	−1.024

Table 4
Chemical hardness (η), vertical ionization potential (VIP) and vertical electron affinity (VEA) of the lowest-energy Si_{n+1} (n = 1–12) and $BaSi_n$ (n = 1–12) clusters.

Cluster	$BaSi_n$			Si_{n+1}			
	η (eV)	VEA (eV)	VIP (eV)	η (eV)	VEA (eV)	VIP (eV)	VIP (eV) (Exp.)
BaSi	5.23	0.46	5.69	6.56	2.05	8.60	>8.49[a]
$BaSi_2$	4.06	1.67	5.73	6.15	2.21	8.37	7.97–8.49[a]
$BaSi_3$	3.89	1.23	5.12	6.03	2.11	8.14	7.97–8.49[a]
$BaSi_4$	3.69	1.84	5.53	6.66	1.51	8.17	7.97–8.49[a]
$BaSi_5$	4.03	2.01	6.04	6.67	1.36	8.02	~7.90[a]
$BaSi_6$	3.80	1.82	5.62	4.95	2.96	7.91	7.46–7.87[a]
$BaSi_7$	3.66	1.86	5.52	5.91	1.74	7.65	7.46–7.87[a]
$BaSi_8$	3.51	2.43	5.94	6.07	1.82	7.89	~7.90[a]
$BaSi_9$	3.71	2.00	5.71	5.79	2.08	7.87	7.46–7.87[a]
$BaSi_{10}$	3.84	2.25	6.09	5.14	2.34	7.48	7.17–7.46[b]
$BaSi_{11}$	3.87	1.96	5.83	4.58	2.68	7.26	7.17–7.46[b]
$BaSi_{12}$	4.01	2.40	6.47	4.95	2.26	7.21	7.17–7.46[b]

[a] Ref. [54].
[b] Ref. [55].

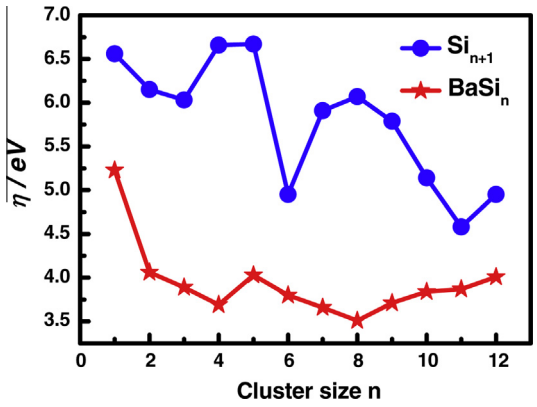

Fig. 5. Size dependence of the chemical hardness η for the lowest-energy structures of $BaSi_n$ and Si_{n+1} clusters.

$$VIP = E_{(\text{cation at optimized neutral geometry})} - E_{(\text{optimized neutral})} \quad (6)$$

$$VEA = E_{(\text{optimized neutral})} - E_{(\text{anion at optimized neutral geometry})} \quad (7)$$

The calculated results of *VIP* and *VEA* are listed in Table 4. From Table 4, we can find that the computational *VIP* values of pure Si_n clusters agree well with the experimental data. In addition, the *VIP* values of $BaSi_n$ clusters are lower than those of pure Si_{n+1} clusters. This means that the doped Ba atom can reduce the stability of Si_{n+1} clusters, which is agree with the above discussion of the $E_b(n)$ and E_{gap}. Furthermore, we can also see that the *VEA* values of $BaSi_n$ clusters increase with the increase of cluster size.

The chemical hardness η is an indicator of the chemical stability, which may be used to characterize the relative stability of molecules and aggregate through the principle of maximum hardness proposed by Pearson [56]. The η can be expressed as

$$\eta = VIP - VEA \quad (8)$$

As illustrated in Fig. 5, we can note that the curves of η for $BaSi_n$ clusters show irregular oscillating behavior, and the two curves have same decrease tendency with the increase of cluster size. For $BaSi_n$ clusters, three local maxima correspond to cluster size with n = 1, 5 and 12, indicating that these clusters are relatively stable than their adjacent clusters. Especially, the BaSi cluster has the largest η value of 5.23 eV, implying that this cluster is extremely inert and may be useful to fabricate the cluster-assembled nanomaterials [30]. The η of the lowest-energy $BaSi_n$ clusters are significantly smaller than those of the corresponding Si_{n+1} clusters. This phenomenon reveals that the doping of Ba atom can enhance metallic characteristics of pure Si_{n+1} clusters.

Infrared and Raman spectra

In order to further determine the stabilities of alkaline earth metal barium doped silicon clusters, it is necessary to analyze the infrared (IR) and Raman spectra of the $BaSi_n$ cluster. The infrared and Raman spectra of magic number $BaSi_5$ are displayed in Fig. 6. From Fig. 6(a), we can see that there are three obvious peaks. The highest intense IR frequency at 285.3 cm^{-1} is assigned to the Si1–Si2 bond in-plane wagging vibration. The double-degenerate intense IR frequency at 348.26 cm^{-1} corresponds to a stretching vibration of the Si4 cluster. The triply degenerate peak at 444.02 cm^{-1} is assigned to the breathing vibration of the Si4 cluster. This IR property is quite different from the experimental IR spectra of pure Si_6 [19] clusters, in which only one strong peak exists at 464 ± 1 cm^{-1}. For the Raman spectra, five strong vibration peaks are found in Fig. 6(b). The strongest vibration peak at

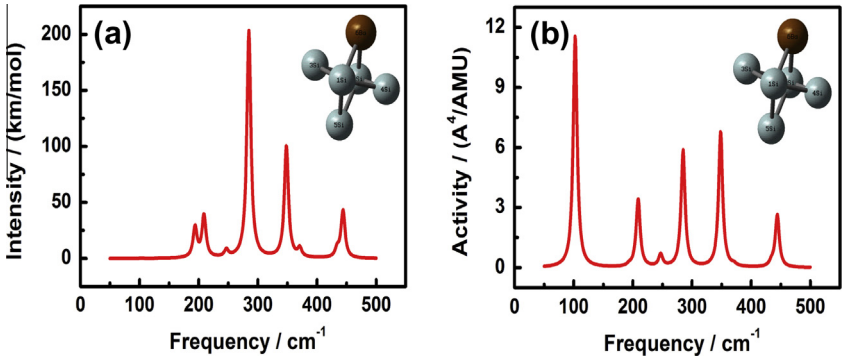

Fig. 6. The infrared (a) and Raman (b) spectra of the $BaSi_5$ cluster.

102.48 cm^{-1} is assigned to the stretching of the Ba atom. The other three strong peaks at 348.26, 285.30, 208.88 cm^{-1} result from the Si3–Si4 bond in-plane stretching, Si1–Si2 bond out-of-plane wagging vibration, and Si3–Si4 bond out-of-plane wagging vibration, respectively. The last vibration peak at 444.02 cm^{-1} is the breathing vibration of the Si4 cluster. These results are similar with the theoretical Raman spectra of YSi_5^- [57] cluster, which has five intense peaks occur at 130, 200, 237, 281 and 309 cm^{-1}, respectively. From Fig. 6, we can also find that the infrared peaks of the $BaSi_5$ cluster are only occur in the high frequency band (285.3–444.02 cm^{-1}), which means that the $BaSi_5$ cluster has stronger infrared activity in the high frequency band. While, the Raman peaks of the $BaSi_5$ cluster are evenly distributed in the whole band, implying that the Raman activity of the $BaSi_5$ cluster are better in the whole band.

Conclusions

The geometries, growth behaviors, relative stability and electronic properties of $BaSi_n$ (n = 1–12) clusters have been systematically investigated at the B3LYP/GENECP level. The results are summarized as follows:

(i) The geometries of silicon clusters are substantially modified after Ba doped. The growth mechanism of the Ba atom doped silicon clusters can be understood as one Si atom capped on $BaSi_{n-1}$ structure or Ba atom capped Si_n structures for different cluster sizes.
(ii) The stability calculated results reveal that $BaSi_n$ clusters with n = 2, 5, 8 and 10 have higher stability than other clusters.
(iii) The Mulliken population analysis indicates that the charge in corresponding $BaSi_n$ clusters transfer from Ba atom to Si atoms. Compared with pure silicon clusters, it is found that a universal narrowing of HOMO–LUMO gap in $BaSi_n$ clusters and the doped Ba atom can reduce the chemical hardness of the pure Si_{n+1} cluster

Acknowledgements

The authors are very grateful for valuable discussions with Professor Maosheng Miao at the University of California, Santa Barbara, USA. This work is supported by the Natural Science Foundation of China (Nos. 11304167 and 51374132), Postdoctoral Science Foundation of China (Nos. 20110491317 and 2014T70280), Young Core Instructor Foundation of Henan Province of China (No. 2012GGJS-152). Open Project of State Key Laboratory of Superhard Materials in Jilin University (No. 201405).

Appendix A. Supplementary material

Supplementary data associated with this article can be found, in the online version, at http://dx.doi.org/10.1016/j.molstruc.2014.06.089.

References

[1] Z.X. Luo, C.J. Grover, A.C. Reber, S.N. Khanna Jr., A.W. Castleman, J. Am. Chem. Soc. 135 (2013) 4307.
[2] Y.S. Wang, S.D. Chao, J. Phys. Chem. A 115 (2011) 1472.
[3] A. Aldongarov, I. Irgibaeva, K. Hermansson, H. Agren, Mol. Phys. 112 (2014) 674.
[4] İ. Muz, M. Atiş, O. Canko, J. Mol. Struct. 1065 (2014) 65.
[5] B.R. Wang, H.Y. Han, Z. Xie, J. Mol. Struct. 1062 (2014) 174.
[6] Y.F. Hu, F.J. Kong, S.J. Wang, Y.Q. Yuan, L.P. Jin, J. Mol. Struct. 1035 (2013) 165.
[7] N.M. Tam, T.B. Tai, M.T. Nguyen, J. Phys. Chem. C 116 (2012) 20086.
[8] H.W. Fan, J.C. Yang, W. Lu, H.M. Ning, Q.C. Zhang, J. Phys. Chem. A 114 (2010) 1218.
[9] P.N. Samanta, K.K. Das, Mol. Phys. 111 (2013) 31.
[10] J.T. Lau, K. Hirsch, P. Klar, A. Langenberg, F. Lofink, R. Richter, J. Rittmann, M. Vogel, V. Zamudio-Bayer, T. Möller, B.V. Issendorff, Phys. Rev. A 79 (2009) 053201.
[11] X.Y. Kong, H.G. Xu, W.J. Zheng, J. Chem. Phys. 137 (2012) 064307.
[12] A. Grubisic, H.P. Wang, Y.J. Ko, K.H. Bowen, J. Chem. Phys. 129 (2008) 054302.
[13] G.F. Zhao, J.M. Sun, Y.Z. Gu, Y.X. Wang, J. Chem. Phys. 131 (2009) 114312.
[14] L.J. Guo, G.F. Zhao, Y.Z. Gu, X. Liu, Z. Zeng, Phys. Rev. B 77 (2008) 195417.
[15] C. Lee, W. Yang, R.G. Parr, Phys. Rev. B 37 (1988) 785.
[16] M.J. Frisch, G.W. Trucks, H.B. Schlegel, G.E. Scuseria, M.A. Robb, J.R. Cheeseman, J.A. Montgomery Jr., T. Vreven, K.N. Kudin, J.C. Burant, J.M. Millam, S.S. Iyengar, J. Tomasi, V. Barone, B. Mennucci, M. Cossi, G. Scalmani, N. Rega, G.A. Petersson, H. Nakatsuji, M. Hada, M. Ehara, K. Toyota, R. Fukuda, J. Hasegawa, M. Ishida, T. Nakajima, Y. Honda, O. Kitao, H. Nakai, M. Klene, X. Li, J.E. Knox, H.P. Hratchian, J.B. Cross, V. Bakken, C. Adamo, J. Jaramillo, R. Gomperts, R.E. Stratmann, O. Yazyev, A.J. Austin, R. Cammi, C. Pomelli, J. Ochterski, P.Y. Ayala, K. Morokuma, G.A. Voth, P. Salvador, J.J. Dannenberg, V.G. Zakrzewski, S. Dapprich, A.D. Daniels, M.C. Strain, O. Farkas, D.K. Malick, A.D. Rabuck, K. Raghavachari, J.B. Foresman, J.V. Ortiz, Q. Cui, A.G. Baboul, S. Clifford, J. Cioslowski, B.B. Stefanov, G. Liu, A. Liashenko, P. Piskorz, I. Komaromi, R.L. Martin, D.J. Fox, T. Keith, M.A. Al-Laham, C.Y. Peng, A. Nanayakkara, M. Challacombe, P.M.W. Gill, B.G. Johnson, W. Chen, M.W. Wong, C. Gonzalez, J.A. Pople, GAUSSIAN 09 Revision C.0, Gaussian Inc., Wallingford, CT, 2009.
[17] J.T. Lyon, P. Gruene, A. Fielicke, G. Meijer, E. Janssens, P. Claes, P. Lievens, J. Am. Chem. Soc. 131 (2009) 1115.
[18] A. Grubisic, Y.J. Ko, H. Wang, K.H. Bowen, J. Am. Chem. Soc. 131 (2009) 10783.
[19] A. Fielicke, J.T. Lyon, M. Haertelt, G. Meijer, P. Claes, J.de. Haeck, P. Lievens, J. Chem. Phys. 131 (2009) 171105.
[20] E.C. Honea, A. Ogura, C.A. Murray, K. Raghavachari, W.O. Sprenger, M.F. Jarrold, W.L. Brown, Nature 366 (1993) 42.
[21] K. Raghavachari, J. Chem. Phys. 84 (1986) 5672.
[22] M. Haertelt, J.T. Lyon, P. Claes, J. de Haeck, P. Lievens, A. Fielicke, J. Chem. Phys. 136 (2012) 064301.
[23] C. Pouchan, D. Bégue, D.Y. Zhang, J. Chem. Phys. 121 (2004) 4628.
[24] M. Vogel, C. Kasigkeit, K. Hirsch, A. Langenberg, J. Rittmann, V. Zamudio-Bayer, A. Kulesza, R. Mitrić, T. Möller, B.V. Issendorff, J.T. Lau, Phys. Rev. B 85 (2012) 195454.
[25] P. Shao, X.Y. Kuang, L.P. Ding, M.M. Zhong, Z.H. Wang, Mol. Phys. 111 (2013) 569.
[26] K.P. Huber, G. Herzberg, Constants of Diatomic Molecules, Van Nostrand Reinhold, New York, 1979.
[27] S. Wengert, J.B. Willems, R. Nesper, Chem. Eur. J. 7 (2001) 15.
[28] S.F. Li, X.L. Xue, G. Chen, D.W. Yuan, Y. Jia, X.G. Gong, J. Chem. Phys. 124 (2006) 224711.
[29] Q. Wang, Q. Sun, J.Z. Yu, B.L. Gu, Y. Kawazoe, Phys. Rev. A 62 (2000) 063203.
[30] P.J. Bruna, S.D. Peyerimhoff, R.J. Buenker, J. Chem. Phys. 72 (1980) 5437.
[31] J.G. Han, C.Y. Xiao, F. Hagelberg, Struct. Chem. 13 (2002) 173.
[32] J.G. Han, F. Hagelberg, J. Mol. Struct: Theochem. 549 (2001) 165.
[33] G. Mpourmpakis, G.E. Froudakis, A.N. Andriotis, M. Menon, Phys. Rev. B 68 (2003) 125407.
[34] F.C. Chuang, Y.Y. Hsieh, C.C. Hsu, M.A. Albao, J. Chem. Phys. 127 (2007) 144313.
[35] B.X. Li, G.Y. Wang, W.F. Ding, X.J. Ren, J.Z. Ye, Phys. B 404 (2009) 1679.
[36] S. Nigam, C. Majumder, S.K. Kulshreshtha, J. Chem. Phys. 125 (2006) 074303.
[37] J.C. Yang, L.H. Lin, Y.S. Zhang, Theor. Chem. Acc. 121 (2008) 83.
[38] D.S. Hao, J.R. Liu, W.G. Wu, J.C. Yang, Theor. Chem. Acc. 124 (2009) 431.
[39] H.W. Fan, Z.Q. Ren, J.C. Yang, D.S. Hao, Q.C. Zhang, J. Mol. Struct: Theochem. 958 (2010) 26.
[40] H.M. Ning, H.W. Fan, J.C. Yang, Comput. Theor. Chem. 976 (2011) 141.
[41] Z.Y. Ren, F. Li, P. Guo, J.G. Han, J. Mol. Struct: Theochem. 718 (2005) 165.
[42] D. Hossain, C.U. Pittman Jr., S.R. Gwaltney, Chem. Phys. Lett. 451 (2008) 93.
[43] P. Guo, Z.Y. Ren, F. Wang, J. Bian, J.G. Han, G.H. Wang, J. Chem. Phys. 121 (2004) 12265.
[44] N.M. Tam, V.T. Ngan, J. de Haeck, S. Bhattacharyya, H.T. Le, E. Janssens, P. Lievens, M.T. Nguyen, J. Chem. Phys. 136 (2012) 024301.
[45] P. Shao, X.Y. Kuang, Y.R. Zhao, H.Q. Wang, Y.F. Li, Mol. Phys. 109 (2011) 315.
[46] D. Die, X.Y. Kuang, J.J. Guo, B.X. Zheng, J. Phys. Chem. Solids 71 (2010) 770.
[47] H.Q. Wang, X.Y. Kuang, H.F. Li, Phys. Chem. Chem. Phys. 12 (2010) 5156.
[48] G.D. Zhou, L.Y. Duan, Structural Chemistry Basis, Peking University Press, Beijing, 2002.
[49] P. Politzer, D.G. Truhlar, Chemical Applications of Atomic and Molecular Electrostatic Potentials, Plenum Press, New York, 1981.
[50] T. Lu, F.W. Chen, J. Comput. Chem. 33 (2012) 580.
[51] R.F.W. Bader, Atoms in Molecules-A Quantum Theory, Oxford University Press, Oxford, 1990.
[52] Y.F. Li, Y. Li, X.Y. Kuang, Eur. Phys. D 67 (2013) 132.
[53] P. Lu, X.Y. Kuang, A.J. Mao, Z.H. Wang, Y.R. Zhao, Mol. Phys. 109 (2011) 2057.
[54] W.A. de Heer, W.D. Knight, M.Y. Chou, M.L. Cohen, Solid State Phys. 40 (1987) 93.
[55] K. Fuke, K. Tsukamoto, F. Misaizu, M. Sanekata, J. Chem. Phys. 99 (1993) 7807.
[56] R.G. Pearson, Chemical Hardness: Applications from Molecules to Solids, Wiley-VCH, Weinheim, 1997.
[57] S. Jaiswal, V.P. Babar, V. Kumar, Phys. Rev. B 88 (2013) 085412.